Eur. Phys. J. D **26**, 231–236 (2003)
DOI: 10.1140/epjd/e2003-00262-x

THE EUROPEAN PHYSICAL JOURNAL D

# Chemical effects on $L_\alpha$, $L_\beta$, $L_\gamma$, $L_l$, and $L_\eta$ X-ray production cross-sections and $L_i/L_\alpha$ X-ray intensity ratios of Hg, Pb and Bi compounds at 59.54 keV

E. Tıraşoğlu[1,a], U. Çevik[1], B. Ertuğral[1], G. Apaydın[1], M. Ertuğrul[2,b], and A.İ. Kobya[1]

[1] Department of Physics, Faculty of Art and Sciences, Karadeniz Technical University, Trabzon, Turkey
[2] Department of Physics, Faculty of Education, Atatürk University, Erzurum, Turkey

Received 7 December 2002 / Received in final form 9 March 2003
Published online 26 August 2003 – 

**Abstract.** Chemical effects on the L X-ray production cross-sections ($\sigma_{L_\alpha}$, $\sigma_{L_\beta}$, $\sigma_{L_\gamma}$, $\sigma_{L_l}$, and $\sigma_{L_\eta}$) and $L_i/L_\alpha$ ($i = \alpha, \beta, l, \eta$) X-ray intensity ratios for Hg, Pb, and Bi compounds were investigated. The samples were excited by 59.54 keV $\gamma$-rays from a $^{241}$Am annular radioactive source. L X-rays emitted by samples were counted by a Si(Li) detector with resolution 157 eV at 5.9 keV. We observed chemical effect on the L X-ray production cross-sections and $L_i/L_\alpha$ X-ray intensity ratios for Hg, Pb and Bi compounds. The experimental values have been compared with the theoretically calculated values of pure elements.

**PACS.** 32.30.Rj X-ray spectra – 32.80.Cy Atomic scattering, cross sections, and form factors; Compton scattering

## 1 Introduction

X-ray emission spectra are known to be influenced by the chemical combination of X-ray emitting atoms with different ligands. The effects of the chemical combination, however, are not large and a theoretical interpretation of these effects has not been established completely. Therefore, chemical effects have rarely been utilized in the characterization of materials.

Reliable values of L X-ray production cross-sections in different elements by photons of various energies are needed because of their wide use in the fields of atomic, molecular and radiation physics and in non-destructive trace elemental analysis of a variety of samples of practical importance using EDXRF. Several studies [1–9] concerned with L X-ray production cross-sections and L X-ray intensity ratios were made. Although effects of excitation mode and excitation energy on L X-ray production cross-sections were studied, there are a few studies [10,11] concerned with chemical effect on L X-ray production cross-sections. $L_i$ X-ray emission lines are caused by transitions as illustrated in Figure 1.

Chemical effects on K and L X-ray intensity ratios and cross-sections are not very well-known. It is also well-known that X-ray spectra depend on the chemical surroundings of the atom. Especially K X-ray intensity ratios and K X-ray production cross-sections of $3d$ elements strongly depend on chemical state. Some studies [12–14] concerned with chemical effects on the $K_\beta/K_\alpha$ intensity ratios and $K_\alpha$ X-ray emission spectra were made. Limited work has been done concerning the chemical effect on L X-ray intensity ratios [15] and L X-ray production cross-sections [10,11]. In the earlier works, the authors calculated only the $L_\alpha$, $L_\beta$, and $L_\gamma$ X-ray production cross-sections. In the present work, we measured again the $L_\alpha$, $L_\beta$, and $L_\gamma$ X-ray production cross-sections and also the $L_l$ and $L_\eta$ lines. We have also measured additional compounds not addressed in previous studies.

## 2 Experimental

The studied compounds were listed in Table 1. The purity of commercially obtained materials was better than 99%. Powder samples were sieved using 400 mesh and prepared by supporting on the scotch tape $\approx 10$ mg/cm$^2$ thickness. The particle sizes were sufficiently small that there was no significant correction to the data.

Measurements were carried out on Hg, Pb and Bi stimulated by 59.54 keV gamma photons emitted by an annular 50 mCi $^{241}$Am radioactive source. The fluorescence L X-rays from the sample were detected by the collimated a Si(Li) detector having a thickness of 3 mm and energy resolution of 147 eV at 5.96 keV. The output from the preamplifier, with a pulse pile-up rejection capability,

[a] e-mail: engint@ktu.edu.tr
[b] *Temporary address*: Oak Ridge National Laboratory, P.O. Box 2008, Bldg. 6010, MS 6354 Oak Ridge, TN 37831-6354, USA.

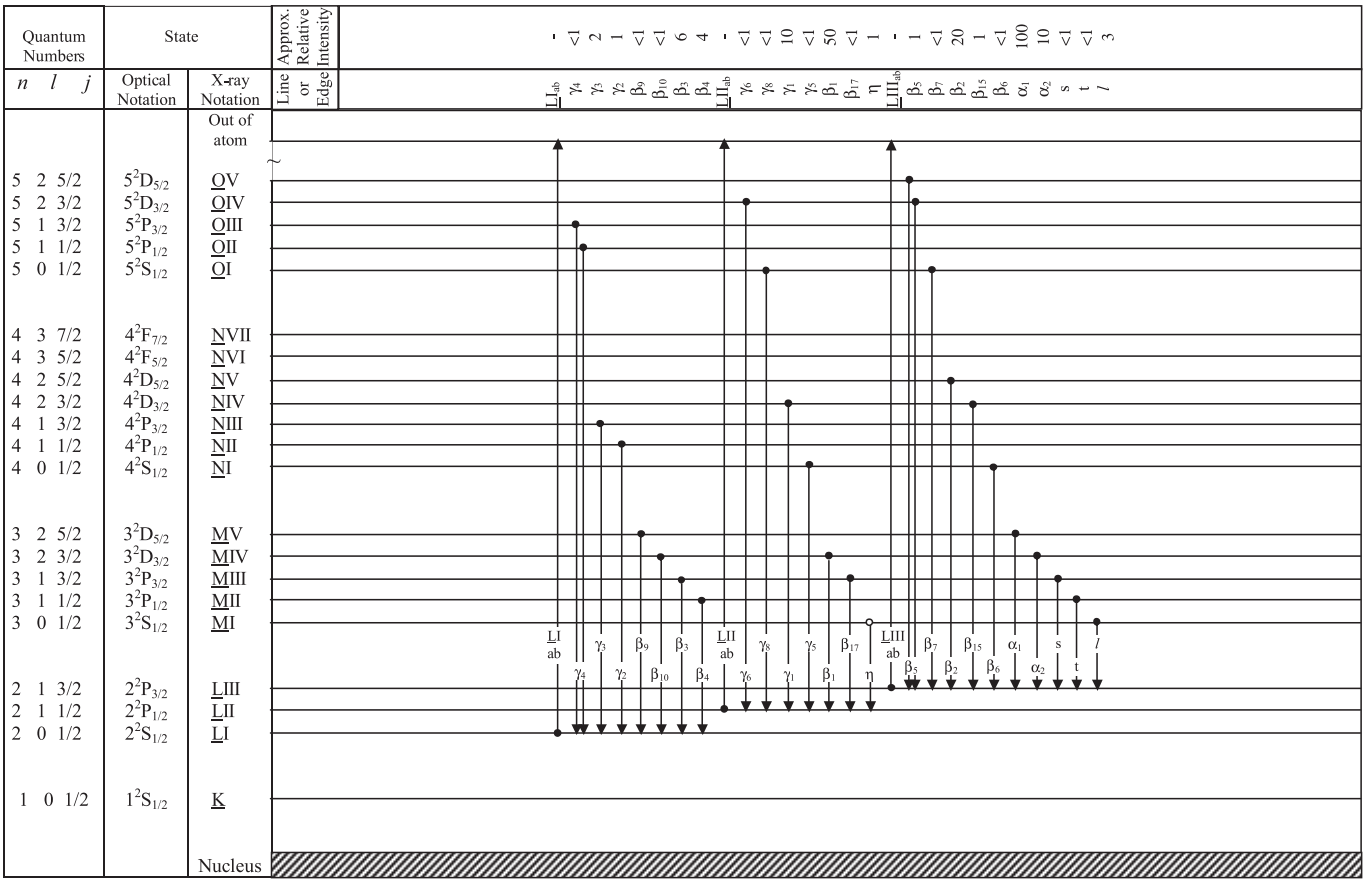


**Fig. 1.** $L_i$ X-ray emission lines.

**Table 1.** The measured values of $\sigma_{L_\alpha}$, $\sigma_{L_\beta}$, $\sigma_{L_\gamma}$, $\sigma_{L_l}$, and $\sigma_{L_\eta}$ production cross-sections (b/atom) of Hg, Pb, and Bi compounds.

| | $\sigma_{L\alpha}$ | | | $\sigma_{L\beta}$ | | | $\sigma_{L\gamma}$ | | | $\sigma_{Ll}$ | | $\sigma_{L\eta}$ | |
|---|---|---|---|---|---|---|---|---|---|---|---|---|---|
| | Theo. | Present | Büyükkasap (1997) | Theo. | Present | Büyükkasap (1997) | Theo. | Present | Büyükkasap (1997) | Theo. | Present | Theo. | Present |
| Hg | 156 | - | - | 158 | - | - | 28.8 | - | - | 8.3 | - | 2.56 | - |
| HgO | | 197±14 | - | | 207±16 | - | | 39±3 | - | | 10.1±0..9 | | 2.58±0.21 |
| $HgSO_3$ | | 114±9 | - | | 131±9 | - | | 24±2 | - | | 6.02±0.56 | | 2.72±0.22 |
| $HgCl_2$ | | 203±16 | 134±11 | | 216±14 | 157±13 | | 35±3 | 37±3 | | 10.8±0.85 | | 2.84±0.22 |
| $HgSO_4$ | | 106±8 | 104±8 | | 125±11 | 122±9 | | 20±2 | 29±2 | | 5.62±0.32 | | 2.62±0.21 |
| $Hg(NO_3)_2$ | | 164±11 | 141±11 | | 179±13 | 170±14 | | 33±3 | 39±3 | | 8.39±0.45 | | 2.03±0.18 |
| $Hg(NO_3)_2.2H_2O$ | | 128±10 | 109±9 | | 144±12 | 129±10 | | 25±2 | 29±2 | | 7.36±0.37 | | 1.85±0.15 |
| $Hg[CH_3CO_2]_2$ | | 146±12 | - | | 158±13 | - | | 29±2 | - | | 7.56±0.38 | | 2.09±0.18 |
| Pb | 192 | 178±13 | 154±12 | 216 | 196±14 | 191±15 | 40.9 | 45±3 | 46±4 | 10.4 | 9.36±0.65 | 3.10 | 2.93±0.20 |
| PbO | | 219±16 | - | | 242±21 | - | | 47±3 | - | | 11.4±0.9 | | 3.05±0.25 |
| $PbO_2$ | | 243±17 | 169±14 | | 266±23 | 210±17 | | 52±4 | 55±4 | | 12.5±1.0 | | 3.15±0.26 |
| $Pb_3O_4$ | | 229±16 | 165±13 | | 254±20 | 197±16 | | 489±4 | 49±3 | | 12.6±0.9 | | 3.09±0.23 |
| $PbCl_2$ | | 217±15 | - | | 231±19 | - | | 471±4 | - | | 12.2±1.0 | | 2.81±0.17 |
| $Pb(NO_3)_2$ | | 184±11 | 144±12 | | 199±15 | 210±17 | | 39±3 | 46±3 | | 9.94±0.78 | | 2.29±0.17 |
| $Pb[CH_3CO_2]_2.3H_2O$ | | 136±10 | 186±15 | | 159±13 | 308±25 | | 30±2 | 65±5 | | 7.22±0.56 | | 1.96±0.14 |
| Bi | 205 | - | - | 217 | - | - | 41.9 | - | - | 11.3 | - | 3.39 | - |
| $Bi_2O_3$ | | 231±18 | 156±12 | | 244±20 | 205±16 | | 46±3 | 41±3 | | 11.8±0.8 | | 3.22±0.21 |
| BiOCl | | 222±17 | 198±16 | | 243±21 | 245±20 | | 501±4 | 62±5 | | 12.8±0.9 | | 3.16±0.22 |
| $Bi_2(CO_3)_3$ | | 275±21 | 237±21 | | 296±24 | 304±24 | | 62±5 | 85±7 | | 15.8±1.1 | | 3.81±0.21 |
| $Bi(NO_3)_3.5H_2O$ | | 126±12 | 237±19 | | 144±12 | 303±24 | | 28±2 | 69±6 | | 6.87±0.45 | | 1.85±0.11 |
| $Bi[CH_3CO_2]_3$ | | 130±10 | - | | 193±16 | - | | 37±3 | - | | 8.81±0.51 | | 2.35±0.16 |

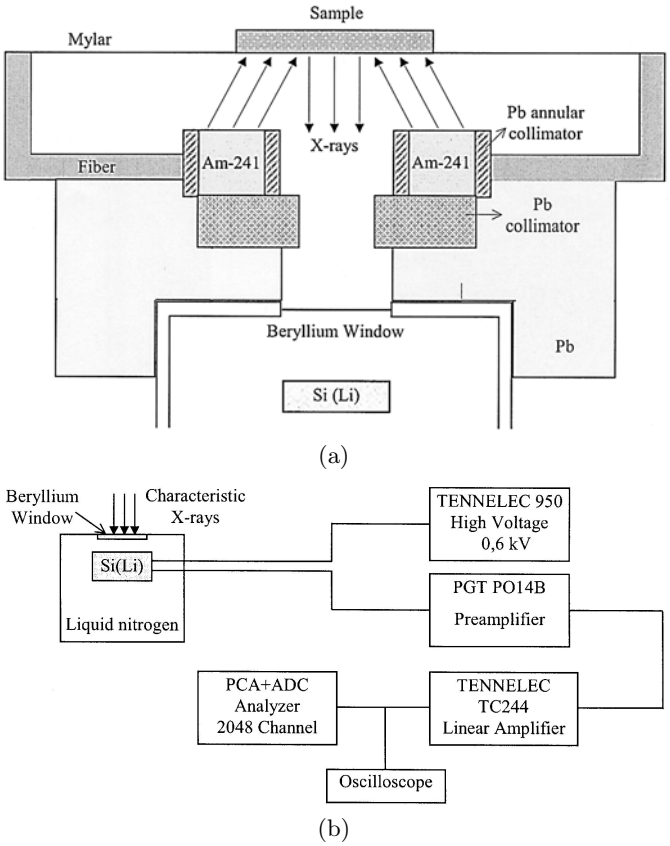


**Fig. 2.** (a) Geometry of the experimental set-up and (b) block diagram of the counting system.

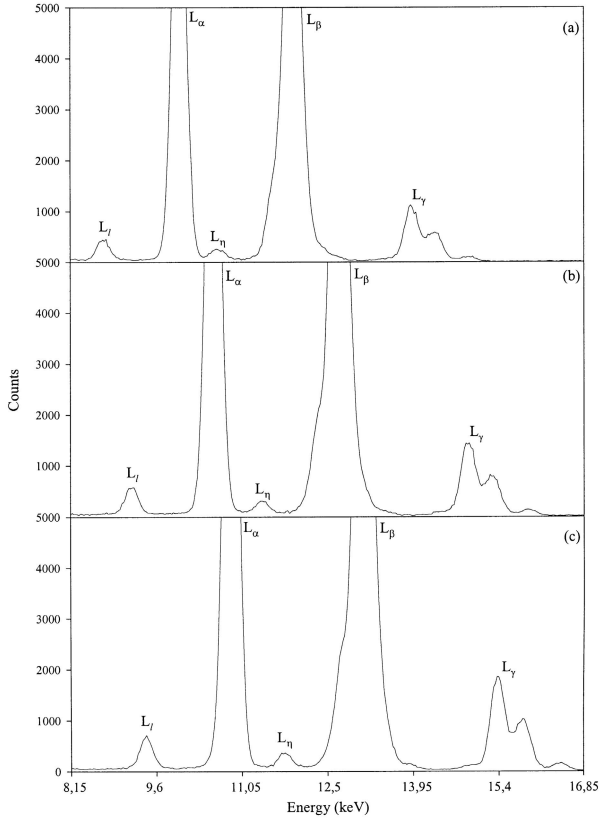


**Fig. 3.** X-ray spectra of the (a) $Hg(NO_3)_2$, (b) $PbO_2$, and (c) $Bi_2O_3$.

was fed to a multi-channel analyzer interfaced with a personal computer provided with suitable software for data acquisition and peak analysis. Spectra were analyzed using the NUCLEUS program (Tennelec, Oak Ridge).

The geometry of the experimental set-up and L X-ray spectra of $Bi_2O_3$, $Hg(NO_3)_2$ and $PbO_2$ in the present study are shown in Figures 2 and 3 respectively. Since fiber consist of C, H and O it does not contribute to the measured spectra.

The $L_\alpha$, $L_\beta$, $L_\gamma$, $L_l$, and $L_\eta$ X-ray production cross-sections have been obtained using the relation [3–5]

$$\sigma_{L_i} = \frac{N_{L_i}}{I_0 G \varepsilon_{L_i} \beta_{L_i} m_i} \tag{1}$$

where $N_{L_i}$ is the measured intensity (area under the photopeak) corresponding to the $L_i$ group of X-rays, $I_0$ is the intensity of the incident radiation, $G$ is a geometrical factor, $\varepsilon_{L_i}$ is the detection efficiency for the $L_i$ group of X-rays and $\beta_{L_i}$ is the self-absorption correction factor for the target material, which accounts for the absorption in the target of the incident photons and the emitted characteristic X-rays. $m_i$ is the thickness of the target in g/cm$^2$.

The experimental L-shell X-ray intensity ratios $I_{L_i}/I_{L_\alpha}$ were evaluated using the relation [6]

$$\frac{I_{L_i}}{I_{L_\alpha}} = \frac{N_{L_i}}{N_{L_\alpha}} \frac{\beta_{L_\alpha}}{\beta_{L_i}} \frac{\varepsilon_{L_\alpha}}{\varepsilon_{L_i}} \quad (i = \beta, \gamma, l, \eta) \tag{2}$$

where $N_{L_i}/N_{L_\alpha}$ represents the ratio of the counting rates under the $L_i$ and $L_\alpha$ peak, $\beta_{L_\alpha}/\beta_{L_i}$ is the ratio of self-absorption correction factors of the target that accounts for the absorption of incident photons and emitted L X-ray photons, and $\varepsilon_{L_\alpha}/\varepsilon_{L_i}$ is the ratio of the detector efficiency values for $L_\alpha$ and $L_i$ X-rays respectively.

The self absorption correction was calculated using the equation

$$\beta = \frac{1 - \exp\{[-(\mu_{\rm inc}\csc\psi_1 + \mu_{\rm emt}\csc\psi_2)m_i]\}}{(\mu_{\rm inc}\csc\psi_1 + \mu_{\rm emt}\csc\psi_2)m_i} \tag{3}$$

where $\mu_{\rm inc}$ and $\mu_{\rm emt}$ are the mass attenuation coefficients (cm$^2$/g) of incident photons and emitted characteristic X-rays respectively [16]; the angles of incident photons and emitted X-rays with respect to the surface of the samples $\psi_1$ and $\psi_2$, were equal to 45° and 90° in the present set-up respectively. The product $I_0 G\varepsilon$, containing the terms related to the incident photon flux, geometrical factor and absolute efficiency of the X-ray detector, was determined by collecting the $K_\alpha$ and $K_\beta$ X-ray spectra of samples of Ca, V, Co, Cu, Y, Mo, Cd, Te, Ba, Nd and Tb in the same geometry and using the equation

$$I_0 G \varepsilon_{K_i} = \frac{I_{K_i}}{\sigma_{K_i} \beta_{K_i} m_i} \tag{4}$$

where $I_{K_i}$, and $\varepsilon_{K_i}$ have the same meaning as in equation (1) except that they correspond to K X-rays instead

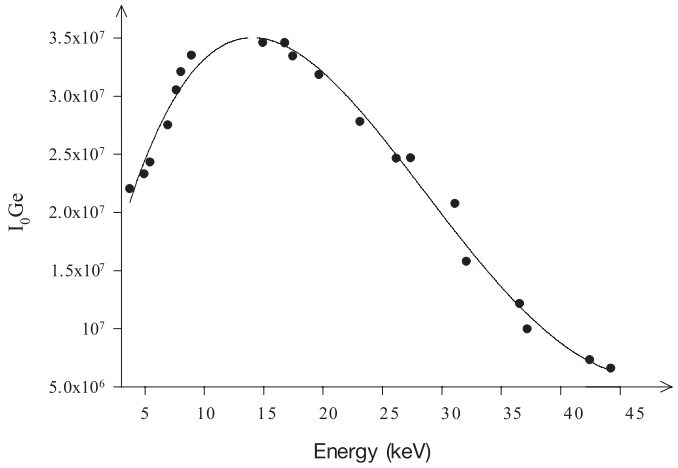


**Fig. 4.** The variation of the factor $I_0G\varepsilon$ as a function of the mean K X-ray energy.

of the $i$th group of L X-rays. Moreover, the self absorption correction has been calculated for compounds.

The mass attenuation coefficients for the compounds are estimated using the elemental values in the following Bragg's rule formula:

$$\mu/\rho = \sum_i \omega_i \mu_i/\rho_i \tag{5}$$

where $\omega_i$ is the proportion by weight of the $i$th constituent and $\mu_i/\rho_i$ is the mass attenuation coefficient for the $i$th constituent in the compound. Theoretical values of $\sigma_{K_\alpha}$ X-ray production cross-sections were calculated using the equation

$$\sigma_{K_i} = \sigma_K(E)\omega_K F_{K_i} \tag{6}$$

where $\sigma_K(E)$ is the K-shell photoionization cross-section of the given element for the excitation energy $E$ [17], $\omega_K$ is the K-shell fluorescence yield [18] and $F_{K_i}$ is the fractional X-rays emission rate for $K_\alpha$ and $K_\beta$ X-rays and is defined as

$$F_{K_\alpha} = \frac{I_{K_\alpha}}{I_{K_\alpha} + I_{K_\beta}} \quad \text{and} \quad F_{K_\beta} = \frac{I_{K_\beta}}{I_{K_\alpha} + I_{K_\beta}} \tag{7}$$

where $I_{K_\alpha}$ and $I_{K_\beta}$ are the $K_\alpha$ and $K_\beta$ X-ray intensities, respectively [19]. The factor $I_0G\varepsilon_{K_i}$ was fitted as a function of energy using the equation

$$I_0G\varepsilon_{K_i} = A_0 + A_1E_x + A_2E_x^2 + A_3E_x^3 + A_4E_x^4 \tag{8}$$

where $E_x$ is the $K_\alpha$ and $K_\beta$ X-ray energy and $A_0$, $A_1$, $A_2$, $A_3$ and $A_4$ are constants evaluated from a fitting polynomial. The variation of the factor $I_0G\varepsilon_{K_i}$ as a function of the mean K X-ray energy is shown in Figure 4.

The values of the factor $I_0G\varepsilon_{L_i}$ for each L X-ray line of average energy $E_{L_i}$ are interpolated from equation (8).

## 3 Results and discussion

The measured values of $\sigma_{L_\alpha}$, $\sigma_{L_\beta}$, $\sigma_{L_\gamma}$, $\sigma_{L_l}$, and $\sigma_{L_\eta}$ production cross-sections of Hg, Pb and Bi compounds at 59.54 keV excitation energy are given in Table 1. In addition, the experimental L-shell X-ray intensity ratios $I_{L_i}/I_{L_\alpha}$ were measured for the above mentioned Hg, Pb and Bi compounds and theoretically calculated for pure elements, and the results are given in Table 2. The theoretical $I_{L_i}/I_{L_\alpha}$ X-ray intensity ratios of pure elements were determined by using the L X-ray fluorescence cross-sections ratios, $\sigma_{L_i}/\sigma_{L_\alpha}$ The values of $\sigma_{L_\alpha}$, $\sigma_{L_\beta}$, $\sigma_{L_\gamma}$, $\sigma_{L_l}$, and $\sigma_{L_\eta}$ production cross-sections are calculated from theoretical values of L subshell photoionisation cross-sections [17] and radiative decay rates [20], semiempirically fitted values of fluorescence yields [21] and Coster-Kronig transition probabilities [21] using the following relations

$$\begin{aligned}
\sigma_{L_l} &= (\sigma_{L_1} f_{13} + \sigma_{L_1} f_{12} f_{23} + \sigma_{L_2} f_{23} + \sigma_{L_3})\omega_3 F_{3l} \\
\sigma_{L_\alpha} &= (\sigma_{L_1} f_{13} + \sigma_{L_1} f_{12} f_{23} + \sigma_{L_2} f_{23} + \sigma_{L_3})\omega_3 F_{3\alpha} \\
\sigma_{L_\eta} &= \sigma_{L_2}\omega_2 F_{2\eta} + \sigma_{L_1} f_{12}\omega_2 F_{2\eta} \\
\sigma_{L_\beta} &= \sigma_{L_1}\omega_1 F_{1\beta} + (\sigma_{L_1} f_{12} + \sigma_{L_2})\omega_2 F_{2\beta} \\
&\quad + (\sigma_{L_1} f_{13} + \sigma_{L_1} f_{12} f_{23} + \sigma_{L_2} f_{23} + \sigma_{L_3})\omega_3 F_{3\beta} \\
\sigma_{L_\gamma} &= \sigma_{L_1}\omega_1 F_{1\gamma} + (\sigma_{L_1} f_{12} + \sigma_{L_2})\omega_2 F_{2\gamma}
\end{aligned} \tag{9}$$

where $\sigma_{L_1}$, $\sigma_{L_2}$ and $\sigma_{L_3}$ are sub-shell photoionization cross-sections of the elements at 59.5 keV; $\omega_1$, $\omega_2$ and $\omega_3$ are the L sub-shell fluorescence yields; $f_{12}$, $f_{13}$, $f_{23}$ are the Coster-Kronig transition probabilities and $F_{ny}$ ($F_{3l}$, $F_{3\alpha}$, $F_{3\beta}$, etc.) are the fractions of the radiation width of the sub-shell $L_n$ ($L_I$, $L_{II}$, $L_{III}$).

The errors in the present measurements are approximately 7–8% and are due to counting statistics, background determination, self-absorption correction and $I_0G\varepsilon$ determination.

As seen from Tables 1 and 2, L X-ray production cross-sections ($\sigma_{L_\alpha}$, $\sigma_{L_\beta}$, $\sigma_{L_\gamma}$, $\sigma_{L_l}$, and $\sigma_{L_\eta}$) are affected by the chemical environment of emitting atom. Matrix element affects the analyte line intensity (or fluorescence cross-sections and intensity ratios) in two ways: as an element (I) out of the molecule and (II) belonging to the molecule containing the L X-ray emitting atom. The effect of the first type can easily be calculated by means of mass attenuation coefficient of atom. The effect of the second type is the most complicated since the individual characteristic structure of molecule affects the L X-ray production cross-sections and L X-ray intensity ratios, both changing the atomic energy levels (or atomic emission rates) and absorbing the emitted photons.

It is well-known that orbital energy levels of L, M, N, O and P shells get closer to each other with increasing quantum number $n$. Outer energy levels are sensitive to the chemical environment by this effect. Thus, outer energy levels are strongly affected by ligands with respect to crystal field theory. These effects play an important role in the $L_\alpha$, $L_\beta$, $L_\gamma$, $L_\eta$, and $L_l$ X-ray transitions and L X-ray production cross-sections. The electron configuration for Hg, Pb, and Bi were given as (Xe)$4f^{14}5d^{10}6s^2$, (Hg)$6p^2$, and (Hg)$6p^3$, respectively. Hg, Pb, and Bi are sensitive to these effects since Hg has an unfilled $6s$ shell, and Pb

**Table 2.** $I_{L_i}/I_{L_\alpha}$ X-ray intensity ratios of Hg, Pb, and Bi compounds.

| | $I_{L\alpha}/I_{L\beta}$ | | | $I_{L\alpha}/I_{L\gamma}$ | | | $I_{L\alpha}/I_{Ll}$ | | $I_{L\alpha}/I_{L\eta}$ | |
|---|---|---|---|---|---|---|---|---|---|---|
| | Theoretical | Present | Büyükkasap 1997 | Theoretical | Present | Büyükkasap 1997 | Theoretical | Present | Theoretical | Present |
| Hg | 0.98 | - | - | 5.42 | - | - | 18.79 | - | 60.94 | - |
| HgO | | 0.94±0.09 | - | | 5.04±0.52 | | | 19.58±2.15 | | 76.9±8.2 |
| $HgSO_3$ | | 0.87±0.09 | - | | 4.67±0.53 | - | | 18.98±2.29 | | 42.1±4.7 |
| $HgCl_2$ | | 0.94±0.09 | 0.85±0.9 | | 5.76±0.66 | 3.62±0.42 | | 18.92±2.10 | | 71.5±7.8 |
| $HgSO_4$ | | 0.84±0.09 | 0.85±0.9 | | 5.28±0.65 | 3.59±0.37 | | 18.89±1.74 | | 40.6±4.5 |
| $Hg(NO_3)_2$ | | 0.91±0.09 | 0.83±0.9 | | 4.94±0.55 | 3.61±0.39 | | 19.59±1.68 | | 81.4±8.8 |
| $Hg(NO_3)_2.2H_2O$ | | 0.88±0.10 | 0.84±0.9 | | 5.03±0.55 | 3.76±0.40 | | 17.42±1.62 | | 69.2±7.7 |
| $Hg[CH_3CO_2]_2$ | | 0.92±0.10 | - | | 5.03±0.54 | - | | 19.42±1.86 | | 70.4±8.3 |
| Pb | 0.89 | 0.87±0.09 | 0.81±0.09 | 4.69 | 5.20±0.51 | 3.35±0.39 | 18.46 | 20.05±2.00 | 61.9 | 66.4±6.6 |
| PbO | | 0.90±0.10 | - | | 4.70±0.45 | - | | 19.33±2.06 | | 72.0±7.8 |
| $PbO_2$ | | 0.91±0.10 | 0.80±0.09 | | 4.68±0.48 | 3.07±0.34 | | 19.56±2.07 | | 77.4±8.5 |
| $Pb_3O_4$ | | 0.90±0.09 | 0.84±0.09 | | 4.73±0.51 | 3.37±0.34 | | 18.25±1.82 | | 74.3±8.0 |
| $PbCl_2$ | | 0.93±0.10 | - | | 4.60±0.50 | - | | 17.78±1.90 | | 77.3±7.1 |
| $Pb(NO_3)_2$ | | 0.92±0.09 | 0.82±0.09 | | 4.65±0.45 | 3.13±0.33 | | 18.56±1.84 | | 80.7±7.6 |
| $Pb[CH_3CO_2]_2.3H_2O$ | | 0.85±0.09 | 0.60±0.07 | | 4.54±0.45 | 2.86±0.32 | | 18.70±2.00 | | 69.8±7.1 |
| Bi | 0.94 | - | | 4.89 | - | - | 18.14 | - | 60.5 | - |
| $Bi_2O_3$ | | 0.95±0.10 | 0.76±0.08 | | 4.97±0.50 | 3.80±0.40 | | 19.52±2.01 | | 68.1±6.9 |
| BiOCl | | 0.83±0.09 | 0.81±0.09 | | 4.02±0.43 | 3.19±0.39 | | 17.34±1.78 | | 64.2±6.61 |
| $Bi_2(CO_3)_3$ | | 0.92±0.10 | - | | 4.45±0.49 | - | | 17.38±1.79 | | 58.2±5.5 |
| $Bi(NO_3)_3.5H_2O$ | | 0.87±0.11 | 0.78±0.08 | | 4.50±0.53 | 3.43±0.40 | | 18.34±2.11 | | 68.1±7.6 |
| $Bi[CH_3CO_2]_3$ | | 0.67±0.08 | | | 3.51±0.38 | | | 14.74±1.41 | | 55.3±5.6 |

and Bi have an unfilled $6p$ shell. On the other hand, because Coster-Kronig transitions include the valence electrons, the chemical effect on the fluorescence cross-sections is due to the chemical effects on the $f_{12}$, $f_{23}$ and $f_{13}$ Coster-Kronig transition probabilities especially for $3d$ elements. The molecules have different bond energies and interatomic distances between the ligands and the central atom because of the oxidation number and the type of the chemical bond. Electron transition probabilities and X-ray production cross-sections may change according to the oxidation number and the type of the chemical bonding when vacancy is created in a shell or a subshell. A change in the chemical bond leads to a change in the valence electron density [22]. When the electron density decreases or increases, some parameters of the atom such as absorption edge energy, photoionization cross-section, also change. So the chemical bonding type such as ionic, metallic, covalent affects the X-ray production cross-sections. The X-ray production cross-sections also depend on the atomic number and the electron configuration of the valence band. It appears that a change in the valence electron density affects the inner shell electron density and distribution. This effect is more important on neighbor electrons according to valence electrons. So we can say that there is an indirect chemical effects on $L_\alpha$, $L_l$ and $L_\eta$ X-rays while there is a direct effect on the $L_\beta$ X-rays. Our results shows that the $L_\beta$ X-rays are affected more by chemical effects.

To obtain more definitive results about chemical effects on the L X-ray production cross-sections, we plan to extend these measurements for various element and various compounds.

This work was supported by Research Fund of Karadeniz Technical University, Trabzon, Turkey, under grant contract No. 20.111.001.6.

## References

1. A. Kaya, M. Ertugrul, O. Dogan, Ö. Söğüt, Ü. Turgut, Ö. Şimşek, Analyt. Chim. Acta **441**, 317 (2001)
2. M. Ertuğrul, Z. Phys. D **38**, 91 (1996)
3. M. Ertuğrul, Analyt. Chim. Acta **454**, 327 (2002)
4. M.K. Garg, S. Kumar, D. Metha, H.R. Verma, P.C. Mengal, P.N. Trehan, J. Phys. B: At. Mol. Phys. **18**, 4529 (1985)
5. E. Tiraşoglu, U. Çevik, B. Ertuğral, Y. Atalay, A.İ. Kopya, Rad. Phys. Chem. **60**, 11 (2001)
6. M. Ertuğrul, Nucl. Instrum. Meth. B **179**, 459 (2001)
7. D.V. Rao, R. Cesareo, G.E. Gigante, X-ray Spectrom. **22**, 401 (1993)
8. M. Ertuğrul, Phys. Scripta **65**, 323 (2002)
9. K.A. Al-Saleh, N.S. Saleh, Rad. Phys. Chem. **54**, 117 (1999)

10. E. Baydaş, Ö. Söğüt, Y. Şahin, E. Büyükkasap, Rad. Phys. Chem. **54**, 217 (1999)
11. E. Büyükkasap, Spectrochim. Acta B **52**, 1167 (1997)
12. F. Folkman, Nucl. Instrum. Meth. B **109/110**, 39 (1996)
13. S. Raj, H.C. Padhi, M. Polasik, Nucl. Instrum. Meth. B **145**, 485 (1998)
14. P.R. Sarode, X-Ray Spectrom. **22**, 138 (1993)
15. E. Baydaş, N. Ekinci, E. Büyükkasap, Y. Şahin, Spectrochim. Acta B **53**, 151 (1998)
16. E. Storm, I. Israel, Nucl. Data Tab. A **7**, 565 (1970)
17. J.H. Scofield, UCRL Report 51326 Lawrence Livermore Laboratory Livermore CA, 1973
18. M.O. Krause, C.W. Nestor, C.J. Sparks, E. Ricci, Oak Ridge Laboratory Report ONRL, 5399 (1978)
19. J.H. Scofield, At. Data Nucl. Data Tab. **14**, 121 (1974)
20. J.H. Scofield, Phys. Rev. A **179**(1), 9 (1969)
21. M.O. Krause, J. Phys. Chem. Data **8**, 377 (1979)
22. Ö. Söğüt, E. Baydas, E. Büyükkasap, A. Küçükonder, Y. Şahin, Eur. Phys. J. D **22**, 13 (2003)